Microchimica Acta (2025) 192:91
https://doi.org/10.1007/s00604-024-06937-6

RESEARCH

Polydopamine-encapsulated carbon dots to boost analytical performance for microplastics detection in fluorescence mode

Keao Liu[1] · Fengshan Liu[1] · Yang Xu[1]

Received: 29 November 2024 / Accepted: 27 December 2024 / Published online: 17 January 2025

Abstract

A kind of sulfur-doped carbon dots was prepared which were encapsulated with polydopamine (S-CDs@PDA) that has fluorescence response on polyethylene (PE) microplastics (MPs). Modified membranes were constructed using S-CDs@PDA for MP detection. Through heating and vacuum filtration process, yellow emission from the modified membrane appeared because of the combination between S-CDs@PDA and PE MPs. Notably, the fluorescence signal value of PE MPs detected by S-CDs@PDA-modified membrane was 21.3% higher than that of unmodified S-CDs membrane, and the detection efficiency was 8% higher than that of S-CDs membrane. The minimum detection limit for modified membranes was 4 mg. Due to the good adhesion of polydopamine (PDA), S-CDs@PDA-modified membrane was more easily adhered to PE MPs, showing its excellent detection ability. The rapid quantitative detection of PE MPs in 10 min was realized with a linear equation of $y = 3081x + 3686.1$ in a linear range of 4–14 mg. Such modified membrane exhibited excellent anti-photobleaching using continuous 365-nm excitation and its sensing performance was further confirmed in sea and river water samples. S-CDs@PDA could detect solid MP powders as well as MPs dispersed in liquids. The detection method constructed with a modified glass fiber filter membrane enables rapid identification and quantitative detection of PE MPs without relying on large-scale instrumentation. This study provided research ideas for fluorescent tracing of PE MPs and paved the way for quantitative detection of micron-sized plastics with smaller particle sizes.

Keywords Polydopamine · Carbon dots · Modified membranes · Microplastic · Fluorescent sensors

Introduction

Plastic is a synthetic polymer compound that has become an indispensable material in human life today and is widely used in household appliances, automobile parts, children's toys, and other aspects [1]. Tons of plastic products are consumed globally every year, with studies suggesting that by 2025 it could reach around 600 million tons [2]. As the use of plastics increases, large amounts of plastics are discarded every day. These discarded plastics are harmful to human health and the ecosystem [3]. When plastics are exposed to the environment, due to physicochemical and other effects, they turn into plastic fragments, which are considered MPs when they are less than 5 mm in size [4, 5]. The first studies on MPs were first reported in 1972 by E. J. Carpenter and K. L. Smith [6]. MPs can be divided into primary and secondary MPs depending on their source. Plastic products derived from direct production are primary MPs, which have specific functions and applications. Secondary MPs are produced from plastics that are exposed and abandoned in the environment through a variety of actions such as light, abrasion or microbial decomposition [7]. MPs are small in size, are easily dispersed, and have been detected in oceans [8–10], freshwater and drinking water [11], and air [12]. The small size of MPs makes it difficult to find them with the naked eye, especially when they are dispersed in a medium. In addition, the hydrophobicity of MPs makes detection even more difficult [13]. These are problems that need to be solved in order to detect MPs. Currently, Raman spectroscopy [14], peptide-modified microneedles [15], thermal imaging [16], pyrolysis gas chromatography coupled with mass spectrometry (GC–MS) [17],

✉ Yang Xu
xyang@hebut.edu.cn

[1] School of Chemical Engineering and Technology, Hebei Key Laboratory of Functional Polymers, Hebei University of Technology, Beichen District, Xiping Road No. 5340, Tianjin 300401, China

liquid chromatography (LC) [18], and Fourier transform infrared spectroscopy (FT-IR) [19] have been applied to the detection of MPs. However, these methods require the support of expensive instruments, as well as a lot of energy and time for experimental testing [20]. To overcome these challenges, staining MPs with fluorescent dyes has been proposed as a way to improve detectability and selectivity [21]. Nile red [22] and rhodamine B [23] have been used to identify MPs by fluorescent staining. Nevertheless, these fluorescent dyes have the potential to stain natural organic matter, which can result in false positive signals [24]. Additionally, the fluorescence is susceptible to background interference [25]. In the absence of complete removal of the interfering organic matter, the staining method cannot be employed as a independent technique, thereby limiting the scope of fluorescence detection. The background and false positive signals represent significant challenges in the study of MPs in fluorescence mode. The activation of fluorescence analysis serves to reduce background interference and facilitate the reflection of real samples [26]. Carbon nanomaterials have the properties of nanomaterials with optical stability and wavelength-dependent photoluminescence (PL) and can be used as fluorescent probes for detection [27].

Carbon dots (CDs) are emerging as a prominent contender in the field of nanomaterials, largely due to their exceptional adsorption and optical characteristics [28]. Due to their unique properties, CDs have been used in metal ion detection [29, 30], photovoltaics [31], and solar cells [32]. Kawan F. Kayani and his colleagues also discussed for the first time the need for future development of CD-based glucose (Glu) sensors through a comprehensive introduction to Glu and CDs [33]. Recent studies have demonstrated the affinity of carbon nanomaterials for MPs [34], and it has also been suggested that MPs can be detected using PL from CDs [35]. In order to make full use of the excellent optical properties of CDs, some studies have proposed the application of CDs to fluorescent sensors [36, 37].

Fluorescence sensors are more suitable as fast and sensitive tools than traditional mass spectrometry or chromatography methods [38]. Among the various techniques developed in the last decade, imaging of MPs using fluorescence sensing (which emits fluorescence upon excitation at specific wavelengths) has gained wider application due to its ease of application and the ability to customize different solvents for higher selectivity [39]. At the same time, fluorescence sensors allow for the visual detection of the target. Visual detection is a straightforward method that produces discernible outcomes, offering the benefits of minimal instrumentation expense, rapid detection, simplicity of operation, reduced consumption of samples and reagents, and the capacity for on-site analytical transferability [40]. Therefore, from a practical point of view, the development of a portable analytical tool for field analysis is essential.

Paper-based sensors (PADs) show great promise for detection and analysis. PADs offer the advantages of low cost, convenience, portability, expandability, and environmental friendliness [41], and they enable immediate and on-site detection. A variety of paper-based sensors have been prepared including nucleic acid biosensors [42], respiratory analysis sensors [43], textile sensors [44], and capacitive touch sensors [45]. Based on these applications and the advantages of paper-based sensors, the combination of fluorescence detection and PADs for the detection of MPs is a viable approach. The small particle size of S-CDs can only fluorescently identify PE MPs, and the fluorescence recognition of MPs using S-CDs may not be effective when the MP content in the sample is low. Therefore, encapsulation of S-CDs by materials with excellent adhesion properties can achieve fluorescent labelling of S-CDs by adhering traces of MPs. Tushar Kanti Das and his colleagues investigated 2D composite nanomaterial membranes for the capture and removal of trace MPs [46]. Inspired by this, the development of fluorescent PADs using CDs composite nanomaterials with good adhesion properties can detect trace MPs in real samples. Previous studies have shown that polydopamine (PDA) is one of the simplest and most versatile methods of functionalizing material surfaces [47]. PDA formed by the self-polymerization of dopamine can impart excellent adhesion properties to materials.

Dopamine is structurally similar to 3,4-dihydroxyphenyl-L-alanine (DOPA) in that both contain catechol and an amino group. In 2007, Haeshin Lee and Phillip B. Messersmith et al. developed a simple and universal surface modification method using dopamine, dopamine oxidative self-polymerisation reaction [48]. PDA has the characteristics of strong adhesion and easy modification, etc. PDA can be adhered to the surface of materials or particles for surface modification to give the material new properties, which is a very promising application. PDA modification can facilitate the transformation of a wide range of material properties [49–52] and has been used in biomedical [53] and industrial wastewater treatment applications [54]. Due to the strong adhesion properties conferred by PDA to the material, PDA has also been widely applied as an adhesive for the adsorption and recovery of MPs in recent years [55, 56]. However, there are very few reports on the application of PDA utilizing its excellent adhesive properties for adsorption detection of MPs by directly applying it to construct fluorescent sensors.

The aim of this work is to utilize the adhesion properties of PDA and the fluorescent response of S-CDs on PE MPs to construct a complex that not only binds plastics rapidly but also emits a fluorescent response to detect PE MPs. In view of this, we present a strategy for detecting PE MPs using luminescence and removing PE MPs using adhesion. A kind

of composite (S-CDs@PDA) was synthesized by encapsulating dopamine on the surface of S-CDs using self-polymerization of dopamine. PDA is non-toxic and endows S-CDs@PDA with good biocompatibility. The loaded PDA enhanced the hydrophobicity of S-CDs, which made PE MPs easier to be detected, fluoresced within 10 min of S-CDs@PDA binding to PE MPs. What's more, S-CDs@PDA has better adhesion and is easier to bind to MPs. Conventional filter paper can only retain plastics with large particle sizes, but is less effective in retaining plastics with micron or nanometer sizes. We also prepared a low-cost, fast-detecting fluorescent sensor by loading S-CDs@PDA onto a glass fiber filter membrane with a pore size of 0.33 μm. The fluorescent filter cake was vacuum filtered for 7 min, then heated in an oven at 60 °C for 3 min, and the image of the filter cake was captured by a smartphone. The images were then analyzed and calculated using ImageJ processing software. On this basis, a linear equation with the range of 4–14 mg was observed to realize the rapid quantitative detection of PE MPs. Because of the excellent adhesion of S-CDs@PDA, it can combine more PE MPs than S-CDs, enhancing the retention rate of PE MPs. Notably, the fluorescence signal value of PE MPs detected by S-CDs@PDA-modified membrane was 21.3% higher than that of S-CD membrane, and the detection efficiency was 8% higher than that of S-CD membrane. Due to the good adhesion of PDA, the S-CDs@PDA-modified membrane adhered PE MPs more easily and showed excellent detection ability. Comparing the slopes of the linear equations constructed by the two sensors based on S-CDs and S-CDs@PDA, the fluorescence labeling effect of S-CDs@PDA was better than that of the uncoated S-CDs. The sensor based on S-CDs@PDA and membrane is easy to operate. It has high sensitivity, low detection limit, fast detection speed, and few interfering signals, and is able to detect PE MPs effectively.

Experimental section

Chemicals

Pyrene was purchased from Shanghai Aladdin Bio-Chem Technology Co., Ltd. Dithiosalicylic acid was purchased from J&K Scientific. N,N-Dimethylformamide (DMF) and anhydrous ethanol were purchased from Tianjin Damao Chemical Reagent Factory. Concentrated hydrochloric acid, concentrated nitric acid, and tris(hydroxymethyl)aminomethane (Tris) were purchased from Fuchen (Tianjin) Chemical Reagent Co. PE was purchased from Shanghai Runhong International Trade Co., Ltd. Polypropylene (PP) and polyvinyl chloride (PVC) powders were purchased from Shanghai McLean Biochemical Co. Polystyrene (PS) was purchased from Aladdin Bio-Chem Technology Co. Dopamine hydrochloride was purchased from Tianjin Hiens Biochemical Technology Co. Chemical Reagent Co. The glass fiber filter membrane was purchased from Changde Beekman Biotechnology Co. Deionized water was used as the aqueous solution in all this study. All the drugs were not further purified.

Instrumentation

The morphology of S-CDs@PDA was observed by transmission electron microscopy (TEM, Talos F200S) at an accelerating voltage of 200 keV. Fluorescence spectra were collected using a FLS 1000 fluorescence spectrometer manufactured by Edinburgh Instruments. Scanning electron microscopy (SEM, Nova Nano SEM450) was used to characterize the surface morphology of plain membranes, modified membranes, and plastics. FT-IR spectra were obtained on a Shimadzu FTIR spectrophotometer (IRAffinity-1S). X-ray photoelectron spectra (XPS) were obtained using an X-ray photoelectron spectrometer (Thermo Scientific ESCALAB250 Xi). Chengde Dingsheng JY-82C Video Contact Angle Tester is used to characterize the contact angle of S-CDs and S-CDs@PDA with water.

Synthesis of nitropyrene

Nitropyrene was prepared by high-temperature reflux using pyrene as raw material. A total of 500 mg of pyrene was placed in a round-bottom flask, followed by 40 mL of concentrated nitric acid for nitration. The solution was refluxed and stirred in an oil bath at 80 °C for 12 h, cooled to room temperature, diluted the solution with a large amount of deionized water and suction filtration, washed with absolute ethanol first, and then washed with a large amount of deionized water until the filtrate was neutral. The filter cake was dried in an oven at 60 °C to obtain the yellow powder nitropyrene.

Synthesis of S-CDs

S-CDs were synthesized by solvothermal method according to previous literature [57]. First, 14 mg of nitropyrene with 7 mg of dithiosalicylic acid was added to 10 mL of DMF and ultrasonicated for 10 min to dissolve it completely, forming a transparent yellow-green solution. The solution was then transferred to a 30-mL polytetrafluoroethylene high-pressure reactor and placed in an oven for 6 h at a temperature of 200 °C. At the end of the reaction, the solution was cooled to room temperature, then the solution was removed and filtered through a 0.22-μm filter membrane. The filtrate was dispersed in boiling water, pumped and washed, and then the filter cake was dried in an oven at 60 °C to finally obtain S-CDs.

Synthesis of S-CDs@PDA

S-CDs were used as raw materials to prepare S-CDs@PDA by dopamine self-polymerization in situ under weakly alkaline conditions (pH = 8.5). The synthesis process of PDA is referred to other literature [56]. First, 0.9085 g of tris (hydroxymethyl) aminomethane was weighed into a beaker, dissolved by sonication in 75 mL of water, and then the pH was adjusted to 8.5 by the dropwise addition of 12 mol/L of concentrated hydrochloric acid. A total of 85 mg of synthesized S-CDs was weighed and evenly dispersed in the configured Tris–HCl buffer solution by sonication, and the supernatant was centrifuged at 6000 rpm for 5 min in a beaker. Eighty-five milligrams of dopamine hydrochloride was weighed in a beaker and a small amount of water was added to dissolve it, then the dopamine hydrochloride solution was mixed with the supernatant and stirred for 12 h. At the end of the reaction, the solution was centrifuged at 11,000 rpm for 5 min. Finally, the lower sediment in the centrifuge tube was washed three times with water and dried at 80 °C for 8 h. The black powder obtained was S-CDs@PDA.

Preparation of S-CDs@PDA-loaded glass fiber filter membrane

A fluorescent sensor based on a glass fiber filter membrane was proposed to quantitatively evaluate polyethylene porous materials. Five milliliters of S-CDs@PDA ethanol solution (0.5 mg/mL) was in a surface dish, and then a glass fiber filter membrane with a pore size of 0.33 μm was soaked in the surface dish and dried in an oven at 60 °C for 5 min to obtain the S-CDs@PDA-loaded glass fiber filter membrane (PFM). The simple filtration unit consists of a Büchner funnel, a filter flask, and a circulating water vacuum pump. The PFM was added into the Büchner funnel, and then the PE MP aqueous solution was added by suction.

Preparation of S-CDs-loaded glass fiber filter membrane

S-CDs-loaded glass fiber filter membrane (SFM) was prepared in the similar process with PFM, while the adding amount of S-CDs was 3.6 mg to keep the same amount of S-CDs for immersion.

Quantification of PE-MPs by PFM-based fluorescence method

A simple and rapid vacuum distillation process provides a contact opportunity between S-CDs@PDA and PE MPs on the surface of PFM. After filtration, bright yellow fluorescence could be observed under 365-nm excitation because of the surface environment change of S-CDs@PDA in PE matrix. The fluorescence image was obtained by the smartphone photo system including CMOS sensor, ISO-1250, 26-mm focal length, and f/1.6 lens. Filming takes place in a dark box UV analyzer to block light reflections from other objects. The combination of smartphones with paper-based substrates represents a cost-effective solution for on-the-spot analysis, mobility, and the versatile identification of substances [58]. The fluorescence image of filter cake was processed and calculated by using ImageJ software [59]. First, the fluorescent images taken with the ImageJ software were opened and the dimensions were modified so that all images are the same size. The fluorescent image is passed through the color-separated channel, and then the outside of the filter cake is removed from the image using the locking sleeve tool. The same lasso tool was used each time calculating the fluorescent area.

Exploring the effect of vacuum filtration time on fluorescence PFM detection

The vacuum filtration time will affect the contact time between the loaded S-CDs@PDA and PE-MPs, and then affect the fluorescence intensity and luminous area of the filter cake. Therefore, in order to optimize the conditions, the experiments of vacuum filtration for 1 min, 3 min, 5 min, 7 min, and 10 min were carried out respectively. The fluorescence image of filter cake was obtained and analyzed by ImageJ.

Exploring the effect of heating time on fluorescence PFM detection

Due to the fluorescence quenching effect of PDA, the fluorescence intensity was evaluated in different incubation times. The filter cake was placed in an oven at 60 °C for 1 min, 3 min, 5 min, 7 min, and 10 min, and the fluorescence area was photographed and calculated.

A simple and fast fluorescent PE sensor (PFM) was prepared using S-CDs@PDA and a glass fiber filter membrane. Four milligrams, 6 mg, 8 mg, 10 mg, 12 mg, and 14 mg PE MPs were ultrasonically dispersed in 50 mL aqueous solution, and then filtered by suction for 7 min with the prepared PFM. After filtration, the cake was placed in an oven at 60 °C and heated for 3 min. The filter cake was placed in a dark box UV analyzer, the fluorescence image of the filter cake was captured by a smartphone camera, and the fluorescence analysis was performed by ImageJ software. Each experiment was performed three times.

Investigating the fluorescence stability of filter cake

Vacuum filtration and incubation provided sufficient contact between PE MPs and S-CDs@PDA. In order to explore the fluorescence stability of filter cake, the filter cake was continuously irradiated under UV lamp for 10 min, 30 min, 60 min, and 120 min. Then the fluorescence image was captured by a smartphone and the fluorescence image was calculated and analyzed by ImageJ software.

Exploring the reusability of PFM

The reuse of sensors can lead to significant savings in the cost of inspection. The reuse of PFMs was experimentally characterized. Fourteen milligrams of PE MPs was ultrasonically dispersed in 50 mL of deionized water, followed by pumping and heating with PFMs. Fluorescence images of the filter cake were obtained by photographing with a smartphone. The PFMs that had been pump-filtered was washed with deionized water to clean off the PE MPs from the PFMs for next vacuum filtration. The experiment was performed in 5 cycles. The fluorescence area was then analyzed and calculated using Image software.

Comparison of detection performance of PFM and SFM

To explore the effect of PDA on fluorescence sensing, the performance comparison between S-CDs and S-CDs@PDA was performed. Four milligrams, 6 mg, 8 mg, 10 mg, 12 mg, and 14 mg of PE were ultrasonically dispersed in 50 mL of deionized water and the prepared SFM was evacuated for 7 min. After filtration, the filter cake was heated in an oven at 60 °C for 3 min. The fluorescence images were captured by a smartphone and analyzed by Image software.

Investigating the dyeing properties of PFM on different MPs

To evaluate the selectivity of PFM, we investigated fluorescence signals on other MPs, including PP, PVC, and PS.

Detection in actual samples

Seawater from China's Bohai Sea and lake water from Hebei University of Technology were used to test the actual samples according to the same process by adding the standard recovery method.

Eight milligrams, 10 mg, and 12 mg of polyethylene MPs were ultrasonically dispersed in 50 mL of seawater samples and lake water samples, which were then filtered by vacuum extraction with a PFM for 7 min, and then heated in an oven at 60 °C for 3 min. Each experiment was performed three times. Fluorescence images were captured and acquired by a smartphone, and fluorescence area analysis was performed by ImageJ software.

Results and discussion

The morphology of the as-prepared material was observed by TEM. The material S-CDs@PDA was spherical and the average size was about 130 nm (Fig. 1a). High-resolution transmission electron microscopy (HR-TEM) showed that the internal black particles were uniformly composed of tiny carbon nanoparticles with 2.87 ± 0.47 nm size (Fig. S1); the formation of PDA-encapsulated carbon nanoparticles can be therefore confirmed. Further, lattice spacing of the black particles encapsulated at the same time was 0.31 nm (Fig. 1b), which was similar to that of the (002) facet of graphene [60]. Therefore, the formation of PDA-encapsulated carbon nanoparticles was confirmed.

The surface functional groups were analyzed using FT-IR and XPS. As shown in Fig. 1c, the absorption band at 3475 cm^{-1} belongs to the stretching vibration of the –OH bond [61], and the absorption band at 2800 ~ 3500 cm^{-1} belongs to the stretching vibration of the –NH bond [62]. These peaks are attributed to the amino-functional group of the PDA molecule [63]. The bands at 1402 cm^{-1} and 960 ~ 1150 cm^{-1} belong to the tensile vibration of C–N bond and the tensile vibration of C–O bond [57]. The observation of the C=O bond at 1679 cm^{-1} [64] and the observation of the C–S– bond at 600–700 cm^{-1} [65] proves the existence of S-CDs in the PDA matrix. The XPS full-width spectrum also verified the existence of sulfur in carbon nanoparticles because of the relative atomic contents of 0.34% in XPS characterization (Fig. 1d). Detailed peak fitting of the C1s spectrum of S-CDs@PDA was carried out with four component peaks at 284.73, 285.62, 288.22, and 289.13 eV, corresponding to C–C/C=C, C–O/C–N/C–S, C=O, and O=C–OH functional groups, respectively (Fig. S2a) [66, 67]. The N1s spectrum at 399.12, 400.02, 401.32, and 405.93 eV corresponds to pyridinic N, pyrrolic N, graphic N, and N–O bonds, respectively (Figure S2b) [68, 69]. The partial XPS spectrum of O1s can be divided into two component peaks, with two peaks at 531.72 and 533.02 eV, corresponding to C=O and C–O, respectively (Figure S2c) [70]. In the high-resolution S2p XPS spectra, three ancestral peaks at 163.79, 164.99, and 168.39 eV were attributed to C–S–C, S–S, and C–S–O, respectively, indicating that sulfur was successfully doped in the material (Fig. S2d) [71–73]. The low elemental sulfur content may be due to the encapsulation of the PDA. Therefore, the material in this work was confirmed to be sulfur-doped carbon nanoparticles encapsulated by PDA, which was denoted as S-CDs@PDA.

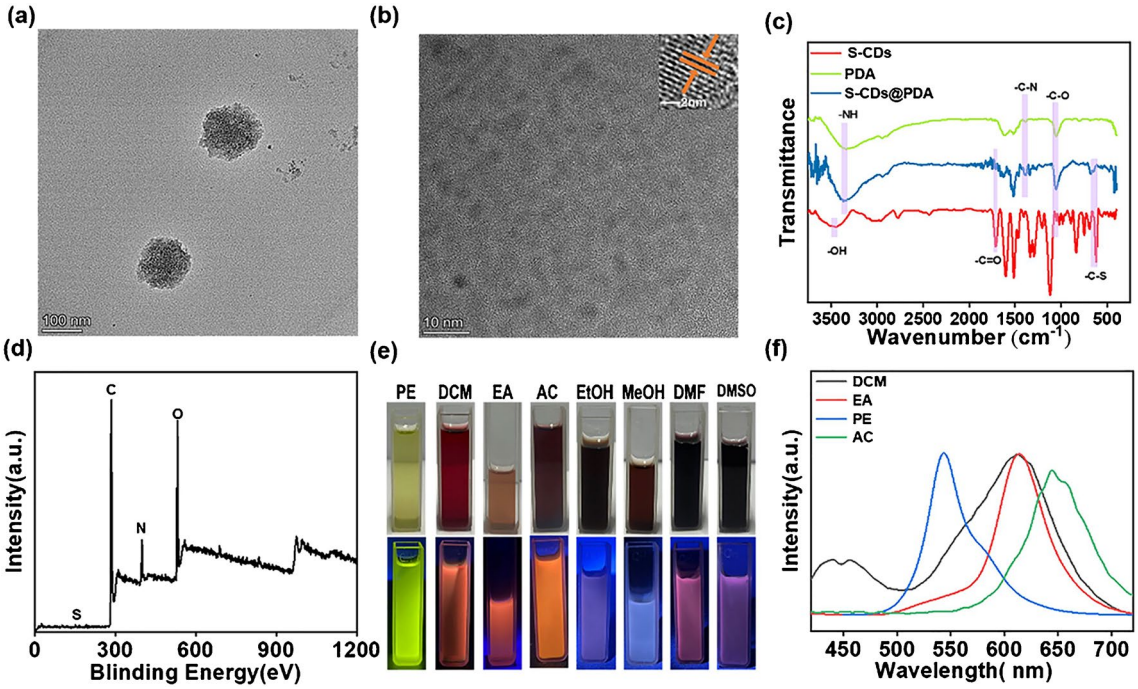

Fig. 1 **a** TEM image of S-CDs@PDA. **b** HRTEM image of S-CDs@PDA. **c** FT-IR spectra of S-CDs, PDA, and S-CDs@PDA. **d** Full spectrum of XPS for S-CDs@PDA. **e** Fluorescence emission plots of S-CDs@PDA in different solvents petroleum ether (PE), dichloromethane (DCM), ethyl acetate (EA), acetone (AC), ethanol (EtOH), methanol (MeOH), DMF, dimethylsulfoxide (DMSO), respectively, from left to right. **f** Fluorescence emission spectra of S-CDs@PDA dissolved in dichloromethane, ethyl acetate, dichloromethane, petroleum ether, and acetone

The polarity of the solvent has a significant effect on the fluorescence of S-CDs@PDA. As shown in Fig. 1e and Fig. 1f, in low-polarity solvents such as petroleum ether, dichloromethane, ethyl acetate, and acetone, the fluorescence of S-CDs@PDA solution is redshifted from green to pink with the increase of solvent polarity. S-CDs fluoresce blue-purple in polar solvents such as ethanol, methanol, DMF, and dimethyl sulfoxide. The results show that S-CDs@PDA has different surface states in different solvents, probably due to the change of surface states caused by the solvent dipole moment, resulting in unique solvent-dependent emission properties [74]. It is proved that S-CDs@PDA inherits the properties of S-CDs [57].

The size of PE MPs was characterized using SEM (Fig. 2a). As shown in Fig. 2b, the calculated average particle size was 6.88 μm. The fluorescence spectra of S-CDs@PDA and PE MPs were characterized (Fig. 2c). Compared to the solid-state fluorescence emission wavelength of the original S-CDs@PDA, a broad peak in the 546–570 nm range was observed for the fluorescence peak of S-CDs@PDA/PE after the addition of PE MPs, but no emission was observed in the blank PE MPs. The reason may be that the contact between S-CDs@PDA and PE passivates the surface states of PE and reduces the density of surface states. Since PL is the result of carrier radiative recombination, which itself is generated by interband leaps of charge carriers, the contact between S-CDs@PDA and PE increases the possibility of radiative recombination via leaps, and thus a fluorescent signal appears [75]. Meanwhile, the quantum yield of S-CDs@PDA/PE was determined to be 4.16% at the optimal excitation wavelength of 365 nm. This indicates that PE MPs affect the surface state of S-CDs@PDA, causing the appearance of fluorescence. This demonstrated that PE MPs could be fluorescently labeled by S-CDs@PDA.

Therefore, PFM was used for quantitative detection of PE MPs. As shown in Fig. 2d and Fig. S3, with the increase of the filtration time, when the filtration time increased from 1 to 7 min, the fluorescence area gradually increased. The fluorescence area tended to stabilize after 7 min of filtration. With the increase of heating time, the fluorescence intensity was enhanced until for 3 min (Fig. 2e and Fig. S4). Therefore, the conditions of filtration time and heating time were determined to be 7 and 3 min, respectively.

The PFM's linear function between the fluorescence area and PE powder quality (Fig. 3) was constructed by using ImageJ software. Figure 2f shows that the linear equation between the fluorescence area and PE mass was $y = 3081x + 3686.05694$ ($R^2 = 0.99269$). Fluorescence analysis is inevitably limited by its low spatial resolution. The MPs were dispersed on the filter paper by vacuum filtration,

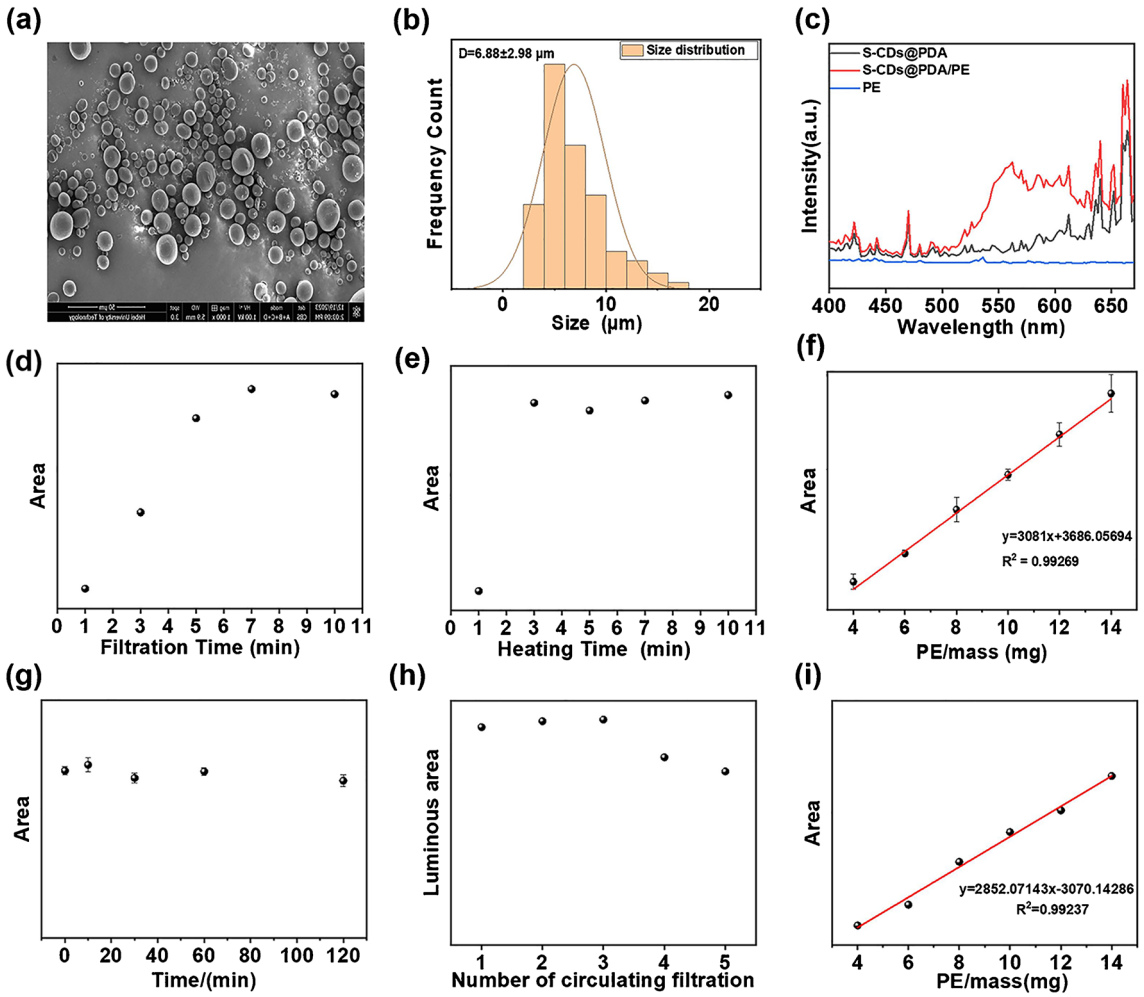

Fig. 2 **a** SEM images of PE MPs. **b** Particle size distribution of PE MPs. **c** Fluorescence images of S-CDs@PDA- and S-CDs@PDA-labeled PE MPs. **d** Relationship between filtering time and fluorescence area. **e** Relationship between heating time and fluorescence area. **f** Linear relationship between the mass of PE MPs (4–14 mg) and the fluorescence area of PFM. (The error bars represent the margin of error for the three sets of parallel experiments.) **g** Equal amount of fluorescence images of PE MPs filtered through PFM and irradiated under 365-nm UV lamp for different times (three sets of parallel experiments). **h** Fluorescence area versus the number of reuse. **i** Linear relationship between PE MP mass (4–14 mg) and fluorescence area of SFM

which effectively reduced the influence of sample depth on fluorescence analysis.

When the filtration was finished, the fluorescence area of PFM and PE MPs mixture did not decrease significantly under the continuous irradiation of UV lamp (Fig. S5). After 120-min irradiation, the fluorescence area decreased to 94.02% of the initial value, indicating that the sensor had excellent anti-photobleaching ability (Fig. 2g). When the PFM was reused five times, the fluorescence area was decreased to 80% of that of the first use (Fig. 2h and Fig. S6). This result demonstrates that the PFM has good reusability, thus saving the cost of MP detection.

In order to compare the detection ability of S-CDs@PDA and S-CDs, the same pumping experiments were performed for SFM as for PFM, and a linear equation was constructed based on the fluorescence area and PE mass of SFM. The linear equation established based on the SFM extraction filter was $y = 2852.07143x - 3070.14286$ with $R^2 = 0.99237$ compared to PFM (Fig. 2i). The fluorescence images of different amounts of PE MPs filtered by SFM are shown in Fig S7. From the linear curve, the slope of PFM is larger than that of SFM. It indicates that the staining efficiency of PE MPs by PDA@S-CDs is higher than that of S-CDs because of strong adhesion of PDA. Therefore, PFM can be used to detect PE MPs when the number of PE MPs is low. Meanwhile, the fluorescence images of filter cake after PFM and SFM filtration were compared. The fluorescence area and fluorescence intensity of PFM were higher than those of SFM. The signal enhancement of PFM may be attributed to hydrophobicity and adhesion of PDA.

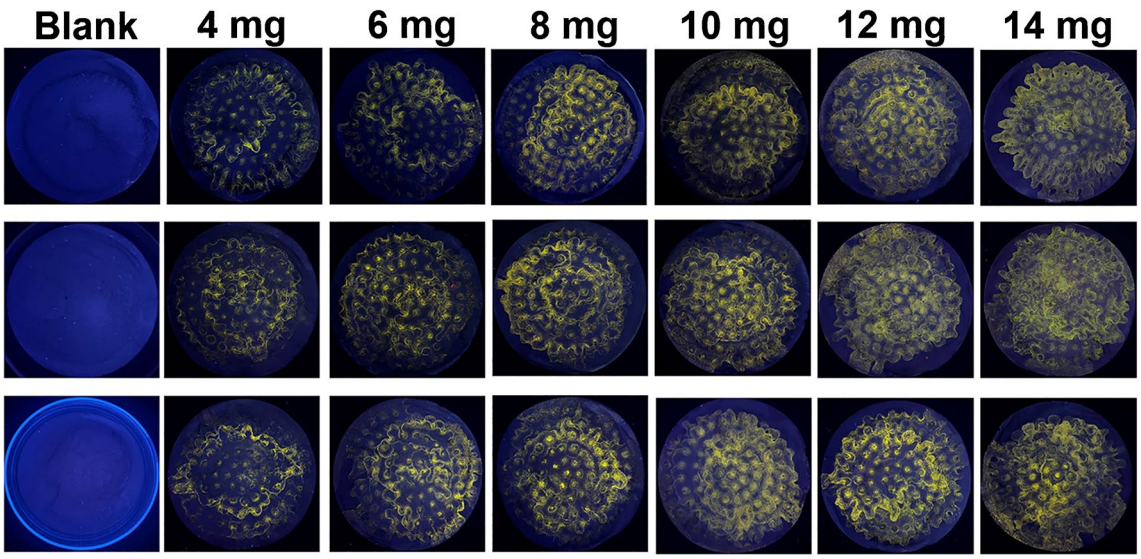

Fig. 3 Fluorescence photographs of different amounts of PE MPs after filtration through PFM (Three sets of parallel experiments)

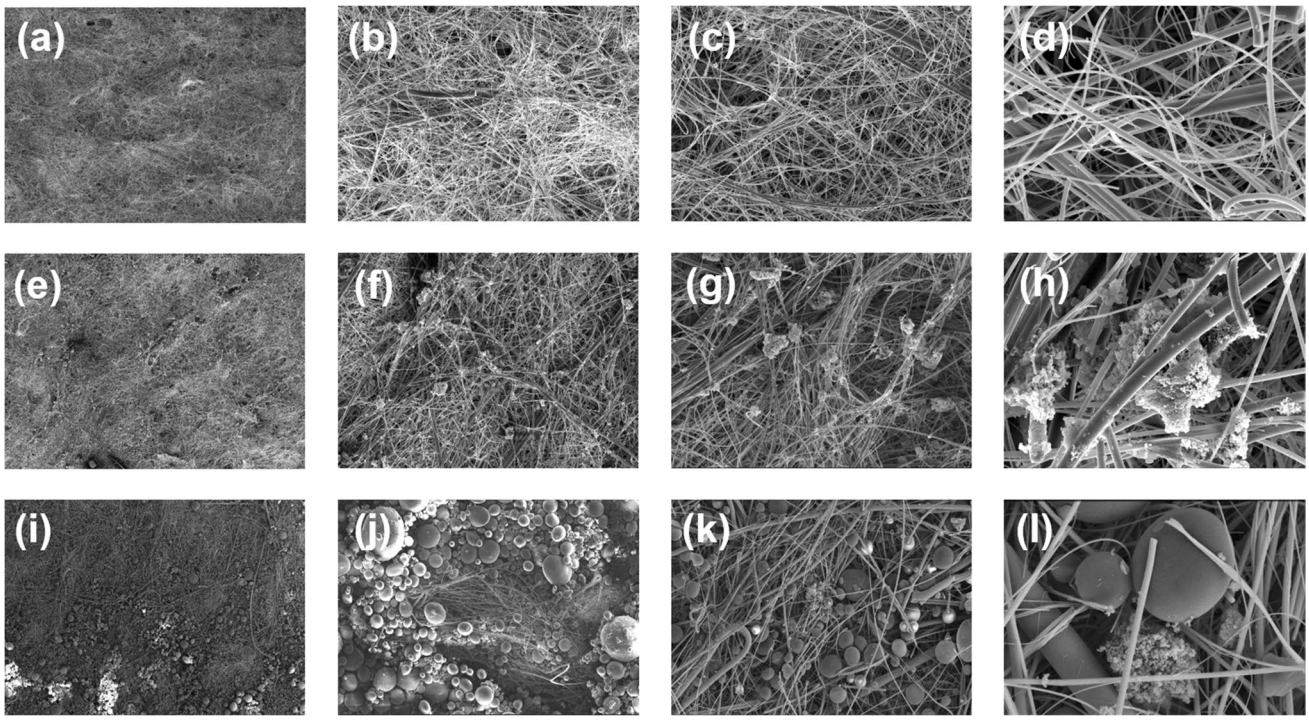

Fig. 4 **a**, **b**, **c**, **d** SEM images of blank membrane at different magnifications. **e**, **f**, **g**, **h** SEM images of modified membrane at different magnifications. **i**, **j**, **k**, **l** SEM images of modified membrane after addition of PE MPs filtration. (From left to right, the four magnifications are 500, 100, 50, and 10 μm.)

To characterize the surface morphology of PFM, SEM was conducted. SEM images of the blank membrane at different magnifications can be seen in Fig. 4a–d. It can be clearly observed that the surface of the membrane consists of longitudinal and transverse fibers. And similar results can be observed in the SEM images of PFM, while S-CDs@PDA dispersed into agglomerates can be seen dispersed on the surface of the membrane and attached to the fibers in the high-magnification SEM images (Fig. 4e–h). Through vacuum filtration, the combination between PE MPs and S-CDs@PDA was achieved, followed with the appearance of fluorescence emission. As shown in

Fig. 4i–l, the filter cake was further characterized by SEM under low and high magnification. In low-magnification image, PE MPs were found to be trapped by the filter membrane. Under high magnification, it was found that the contact between PE MPs and S-CDs@PDA.

To assess selectivity of PFM, a variety of MPs including PP, PVC, and PS were added for vacuum filtration (Fig. S8). PFM did not emit obvious fluorescence signals except PE MPs. The results demonstrated that S-CDs@PDA has excellent selectivity on PE MPs in a short time without complicated pretreatment. To investigate the specific recognition of PE MPs by PFM, PE, PP, PVC, and PS were incubated at 60 ℃ for different times of heating using S-CDs@PDA (Fig. S9). PE MPs emitted yellow fluorescence after incubation. Non-polar PP MPs showed weak fluorescence. As the polarity of the plastic increased, a red shift was observed in the PS and PVC moieties (Fig. S10). This is similar to the fluorescence of S-CDs@PDA solutions in highly polar solvents. Under heating conditions, the diffusion of S-CDs@PDA into the polymer molecules was intensified due to the presence of interstitial spaces in the polymer molecules.

Nevertheless, by regulating the correlation between the incubation reaction time and the fluorescence intensity, a distinction could be discerned between these MPs. Upon mixing and heating S-CDs@PDA and PE MPs for 3 min, a weak yellow fluorescence was observed, whereas the other MPs exhibited minimal bright fluorescence. Furthermore, bright fluorescence was observed in other MPs following heating and incubation for 1 h. Therefore, it is possible to distinguish PE MPs and other MPs from each other based on the presence or absence of fluorescence within a relatively short period of time. As the reaction time increased, PE MPs emitted a stronger yellow fluorescence, while the intensity of the fluorescence emitted by the other MPs remained weak.

In addition, Figure S11 demonstrates the hydrophilicity of S-CDs and S-CDs@PDA. The encapsulation of PDA resulted in enhanced hydrophobicity of the S-CDs, which enhanced the contact with the PE MPs.

In order to investigate the performance of PFM for the detection of PE MPs in real environmental water samples, the practicality of PFM for PE MP detection was evaluated using real environmental water samples in spiked recovery method. In order to exclude the influence of metal ions that may be contained in the actual water samples on the detection, interference experiments with Mn^{2+}, Fe^{3+}, Cu^{2+}, and Al^{3+} were first performed on the PFM (Fig. S12). The concentration of the four metal ions was 1 μM. The results showed that the common metal ions do not affect the fluorescence detection of PFM. The recoveries of this sensing method in seawater and lake samples were ranged from 101.9 to 108% (Table 1 and Fig. S13) and 104.8 to 112.1% (Table 2 and Fig. S14), respectively. These results suggest that the PFM can be used for the detection in real water samples.

Table 1 Determination of MPs in Bohai Sea seawater samples

Added PE (mg)	Found PE (mg)	Recovery (%, $n=3$)	RSD (%, $n=3$)
8	8.15 ± 0.12	101.9%	0.8
10	10.8 ± 0.2	108%	1.6
12	12.5 ± 0.3	104%	2

Table 2 Determination of MPs in lake water samples from Hebei University of Technology

Added PE (mg)	Found PE (mg)	Recovery (%, $n=3$)	RSD (%, $n=3$)
8	8.48 ± 0.49	112.1%	0.2
10	10.71 ± 0.21	109.2%	0.7
12	12.14 ± 0.43	104.8%	1.3

The PFM fluorescence sensor was compared to other sensors (Table S1). The PFM fluorescence sensor is notable for its simplicity of manufacture, its low cost, and its independence from large-scale experimental instruments. It is capable of specific detection of PE MPs in a short time, and can easily meet the detection needs in the actual environment.

Conclusion

S-CDs with special fluorescence response to PE were synthesized by solvothermal method using nitropyrene as carbon source and dithiosalicylic acid as passivator. PDA was synthesized by autoxidation of dopamine in Tris–HCl buffer solution, and the PDA was encapsulated on the surface of S-CDs to form the composite S-CDs@PDA. The complex has good adhesion properties compared to S-CDs. Based on S-CDs@PDA and glass fiber filter membranes, we created a class of paper-based fluorescence sensors and constructed a paper-based fluorescence analysis method combining vacuum pumping filtration and ImageJ analysis for the quantitative evaluation of PE MPs with small particle sizes. There was a significant linear relationship between fluorescence area and PE mass in the range of 4-14 mg.

This study is an investigation on detection of micron-sized plastics in water samples. In addition to MPs dispersed in liquids, solid MP powders can also be detected with S-CDs@PDA. Fluorescence detection of MPs, especially paper-based fluorescent sensors, is a low-cost, easy-to-operate and more convenient detection method compared to other detection methods. Concurrently, the fluorescent sensor can be employed to facilitate real-time on-site detection of PE MPs through visual inspection. In the future, although there has been progress in

the detection and analysis of MPs, there is also a need to focus on the detection of nanoplastics (NPs), which have smaller particle sizes and are more difficult to detect than MPs. Both atomic force microscope (AFM)–based infrared spectroscopy and AFM-based Raman spectroscopy have higher spatial resolution and are promising methods for analyzing NPs [76]. In addition, the combination of nanomaterials and metal–organic frameworks (MOFs) with excellent adsorption capacity for the detection of NPs has great potential for development [77].

Supplementary Information The online version contains supplementary material available at https://doi.org/10.1007/s00604-024-06937-6.

Author contribution Keao Liu: Data curation, Investigation, Writing – original draft.

Fengshan Liu: formal analysis, validation.

Yang Xu: funding acquisition, supervision, writing—review and editing.

Funding This study received financial support from the Hebei Natural Science Foundation (No. B2021202056).

Data Availability Data will be made available on request.

Declarations

Competing interests The authors declare no competing interests.

References

1. Alimi OS, Fadare OO, Okoffo ED (2021) Microplastics in African ecosystems: current knowledge, abundance, associated contaminants, techniques, and research needs. Sci Total Environ 755:142422
2. Liu C, Qiu J, Tang Z, Hu H, Meng F, Li A (2021) Effects of Polystyrene microplastics on growth and toxin production of Alexandrium pacificum. Toxins 13(4):293
3. Sun J, Peng ZT, Zhu ZR, Fu W, Dai XH, Ni BJ (2022) The atmospheric microplastics deposition contributes to microplastic pollution in urban waters. Water Res 225:119116
4. Zhang K, Hamidian AH, Tubić A, Zhang Y, Fang JKH, Wu C, Lam PKS (2021) Understanding plastic degradation and microplastic formation in the environment: a review. Environ Pollut 274:116554
5. Browne MA, Crump P, Niven SJ, Teuten E, Tonkin A, Galloway T, Thompson R (2011) Accumulation of microplastic on shorelines woldwide: sources and sinks. Environ Sci Technol 45(21):9175–9179
6. Carpenter EJ, Anderson SJ, Harvey GR et al (1972) Polystyrene spherules in coastal waters[J]. Science 178(4062):749–750
7. Chen J, Wu J, Sherrell PC, Chen J, Wang H, Zhang WX, Yang J (2022) How to build a microplastics-free environment: strategies for microplastics degradation and plastics recycling. Adv Sci 9(6):2103764
8. Schwarz AE, Ligthart TN, Boukris E, van Harmelen T (2019) Sources, transport, and accumulation of different types of plastic litter in aquatic environments: a review study. Mar Pollut Bull 143:92–100
9. Sun-Kee H (2020) The concept of microplastics and their occurrence, transport, biological effects, and management methods in the ocean. J Environ Health Sci 46(5):610–626
10. Wayman C, Niemann H (2021) The fate of plastic in the ocean environment - a minireview. Environ Sci-Processes Impacts 23(2):198–212
11. Koelmans AA, Nor NHM, Hermsen E, Kooi M, Mintenig SM, De France J (2019) Microplastics in freshwaters and drinking water: critical review and assessment of data quality. Water Res 155:410–422
12. Zhang YL, Kang SC, Allen S, Allen D, Gao TG, Sillanpää M (2020) Atmospheric microplastics: a review on current status and perspectives. Earth Sci Rev 203:103118
13. Wang J, Tao J, Ji J, Wu M, Sun Y, Li J, Gan J (2023) Use of a dual-labeled bioaccumulation method to quantify microplastic vector effects for hydrophobic organic contaminants in soil. ACS Environmental Au 3(4):233–241
14. Iri AH, Shahrah MHA, Ali AM, Qadri SA, Erdem T, Ozdur IT, Icoz K (2021) Optical detection of microplastics in water. Environ Sci Pollut Res 28(45):63860–63866
15. Ahn S, Kim N, Choi Y, Kim J, Hwang H, Kim C, Lee H-Y, Kim S, Kim JS, Lee HH, Choi J (2024) Peptide-decorated microneedles for the detection of microplastics. Biosensors 14(3):140
16. Kedzierski M, Geslain E, Pedrotti ML, Ghiglione JF, Bruzaud S (2021) Pre-detection of microplastics using active thermography. Chemosphere 262:127648
17. Nuelle MT, Dekiff JH, Remy D, Fries E (2014) A new analytical approach for monitoring microplastics in marine sediments. Environ Pollut 184:161–169
18. Elert AM, Becker R, Duemichen E, Eisentraut P, Falkenhagen J, Sturm H, Braun U (2017) Comparison of different methods for MP detection: what can we learn from them, and why asking the right question before measurements matters? Environ Pollut 231:1256–1264
19. Qiu QX, Tan Z, Wang JD, Peng JP, Li MM, Zhan ZW (2016) Extraction, enumeration and identification methods for monitoring microplastics in the environment. Estuar Coast Shelf Sci 176:102–109
20. Li J, Liu H, Paul Chen J (2018) Microplastics in freshwater systems: a review on occurrence, environmental effects, and methods for microplastics detection. Water Res 137:362–374
21. Ho D, Liu SD, Wei HR, Karthikeyan KG (2024) The glowing potential of Nile red for microplastics identification: science and mechanism of fluorescence staining. Microchem J 197:109708
22. Nel HA, Chetwynd AJ, Kelleher L, Lynch I, Mansfield I, Margenat H, Onoja S, Oppenheimer PG, Smith GHS, Krause S (2021) Detection limits are central to improve reporting standards when using Nile red for microplastic quantification. Chemosphere 263:127953
23. Tong HY, Jiang QY, Zhong XC, Hu XS (2021) Rhodamine B dye staining for visualizing microplastics in laboratory-based studies. Environ Sci Pollut Res 28(4):4209–4215
24. Baruah A, Sharma A, Sharma S, Nagraik R (2022) An insight into different microplastic detection methods. Int J Environ Sci Technol 19(6):5721–5730
25. Luo Q, Qin LF, Zhang P, Feng B, Ye XS, Qing TP, Qing ZH (2022) A persistent luminescent nanobeacon for practical detection of lead ions via avoiding background interference. Anal Chim Acta 1198:339555
26. Zhang JQ, Li HH, Li YR, Li SS, Xu Y, Li HR (2022) Boron-doped carbon nanoparticles for identification and tracing of microplastics in "Turn-on" fluorescence mode. Chem Eng J 435:135075
27. Das P, Ganguly S, Rosenkranz A, Wang B, Yu JH, Srinivasan S, Rajabzadeh AR (2023) MXene/0D nanocomposite architectures: design, properties and emerging applications. Materials Today Nano 24:100428

28. Kayani KF, Mohammed SJ, Ghafoor D, Rahim MK, Ahmed HR (2024) Carbon dot as fluorescence sensor for glutathione in human serum samples: a review. Materials Advances 5(11):4618–4633
29. Kayani KF, Shatery OBA, Mustafa MS, Alshatteri AH, Mohammed SJ, Aziz SB (2024) Environmentally sustainable synthesis of whey-based carbon dots for ferric ion detection in human serum and water samples: evaluating the greenness of the method. RSC Adv 14(8):5012–5021
30. Kayani KF, Abdullah CN (2024) A dual-mode detection sensor based on nitrogen-doped carbon dots for visual detection of Fe (III) and ascorbic acid via a smartphone. J Fluorescence 1–13. https://doi.org/10.1007/s10895-024-03604-0
31. Yuan F, Yuan T, Sui L, Wang Z, Xi Z, Li Y, Li X, Fan L, Tan ZA, Chen A, Jin M (2018) Engineering triangular carbon quantum dots with unprecedented narrow bandwidth emission for multicolored LEDs. Nature Commun 9(1):2249
32. Ghann W, Sharma V, Kang H et al (2019) The synthesis and characterization of carbon dots and their application in dye sensitized solar cell[J]. Int J Hydrogen Energy 44(29):14580–14587
33. Kayani KF, Ghafoor D, Mohammed SJ, Shatery OBA (2024) Carbon dots: synthesis, sensing mechanisms, and potential applications as promising materials for glucose sensors. Nanoscale Adv 2024. https://doi.org/10.1039/d4na00763h
34. Tang Y, Zhang SH, Su YL, Wu D, Zhao YP, Xie B (2021) Removal of microplastics from aqueous solutions by magnetic carbon nanotubes. Chem Eng J 406:126804
35. Capolungo C, Genovese D, Montalti M, Rampazzo E, Zaccheroni N, Prodi L (2021) Photoluminescence-based techniques for the detection of micro- and nanoplastics. Chemistry-a Eur J 27(70):17529–17541
36. Lin XF, Xiong MG, Zhang JW, He C, Ma XM, Zhang HF, Kuang Y, Yang M, Huang QT (2021) Carbon dots based on natural resources: synthesis and applications in sensors. Microchem J 160:105604
37. Junaid HM, Solangi AR, Batool M (2021) Carbon dots as naked eye sensors. Analyst 146(8):2463–2474
38. Chen LF, Tian XK, Li Y, Yang C, Huang YJ, Nie YL (2022) Rapid and sensitive screening of multiple polycyclic aromatic hydrocarbons by a reusable fluorescent sensor array. J Hazard Mater 424:127694
39. Sturm MT, Horn H, Schuhen K (2021) The potential of fluorescent dyes-comparative study of Nile red and three derivatives for the detection of microplastics. Anal Bioanal Chem 413(4):1059–1071
40. Kayani KF, Omer KM (2022) A red luminescent europium metal organic framework (Eu-MOF) integrated with a paper strip using smartphone visual detection for determination of folic acid in pharmaceutical formulations. New J Chem 46(17):8152–8161
41. Martinez AW, Phillips ST, Whitesides GM, Carrilho E (2010) Diagnostics for the developing world: microfluidic paper-based analytical devices. Anal Chem 82(1):3–10
42. Wang JS, Davidson JL, Kaur S, Dextre AA, Ranjbaran M, Kamel MS, Athalye SM, Verma MS (2022) Paper-based biosensors for the detection of nucleic acids from pathogens. Biosensors-Basel 12(12):1094
43. Güder F, Ainla A, Redston J, Mosadegh B, Glavan A, Martin TJ, Whitesides GM (2016) Paper-based electrical respiration sensor. Angewandte Chemie-Int Edition 55(19):5727–5732
44. Zhong QZ, Zhong JW, Cheng XF, Yao X, Wang B, Li WB, Wu N, Liu K, Hu B, Zhou J (2015) Paper-based active tactile sensor array. Adv Mater 27(44):7130–7136
45. Mazzeo AD, Kalb WB, Chan L, Killian MG, Bloch JF, Mazzeo BA, Whitesides GM (2012) Paper-based, capacitive touch pads. Adv Mater 24(21):2850–2856
46. Das TK, Basak S, Ganguly S (2024) 2D nanomaterial for microplastic removal: a critical review. Chem Eng J 492:152451
47. Ryu JH, Messersmith PB, Lee H (2018) Polydopamine surface chemistry: a decade of discovery. ACS Appl Mater Interfaces 10(9):7523–7540
48. Lee H, Dellatore SM, Miller WM, Messersmith PB (2007) Mussel-inspired surface chemistry for multifunctional coatings. Science 318(5849):426–430
49. Gu B, Pu GH, Ding BN, Zhang K, He R, Fan JH, Xing T, Wu JY, Yang WB (2022) Improved interfacial bonding strength of silicone rubber/carbon fiber modified by dopamine. Polym Compos 43(10):6975–6986
50. Tian XL, Han S, Zhuang QX, Bian HG, Li SM, Zhang CQ, Wang CS, Han WW (2020) Surface modification of staple carbon fiber by dopamine to reinforce natural latex composite. Polymers 12(4):988
51. Kim HJ, Song JH (2019) Improvement in the mechanical properties of carbon and aramid composites by fiber surface modification using polydopamine. Composites Part B-Eng 160:31–36
52. Xu T, Tian J, An L, Jiao Y, Yin Q, Tan Y (2022) Study on the construction of dopamine/poly (ethyleneimine)/aminoated carbon nanotube multilayer films on aramid fiber surfaces to improve the mechanical properties of aramid fibers/epoxy composites. ACS Omega 7(40):35610–35652
53. Hauser D, Septiadi D, Turner J, Petri-Fink A, Rothen-Rutishauser B (2020) From bioinspired glue to medicine: polydopamine as a biomedical material. Materials 13(7):1730
54. Chen RH, Lin BR, Luo R (2022) Recent progress in polydopamine-based composites for the adsorption and degradation of industrial wastewater treatment. Heliyon 8(12):e12105
55. Peng S, Chen XX, Rong X, Ma HB, Zhao CY, Pang KYJ (2023) Fabrication of eco-friendly Cu/Co-LDHs-based superhydrophobic sponge and efficiently synchronous removal of microplastic, dyestuff, and oil. J Clean Prod 400:136708
56. Chen XX, Ma HB, Ji XY, Han RM, Pang K, Yang ZM, Liu ZM, Peng S (2023) Engineering green MOF-based superhydrophobic sponge for efficiently synchronous removal of microplastics and pesticides from high-salinity water. Water Res 243:120314
57. Li HH, Li YR, Liu FS, Xu Y, Li HR (2023) Identification and quantification of polyethylene microplastics with sulfur-doped carbon nanoparticles in fluorescence mode and construction of paper-based analytical method. Sensors and Actuators B-Chemical 394:134340
58. Kayani KF, Mohammed SJ, Mohammad NN, Abdullah GH, Kader DA, Mustafa NSH (2024) Ratiometric fluorescence detection of tetracycline in milk and tap water with smartphone assistance for visual pH sensing using innovative dual-emissive phosphorus-doped carbon dots. Food Control 164:110611
59. Liu XR, He CN, Huang Q, Yu MM, Qiu Z, Cheng HX, Yang YF, Hao X, Wang XL (2022) A facile visualized solid-phase detection of virus-specific nucleic acid sequences through an upconversion activated linear luminescence recovery process. Analyst 147(11):2378–2387
60. Baker SN, Baker GA (2010) Luminescent carbon nanodots: emergent nanolights. Angew Chem Int Ed 49(38):6726–6744
61. Wang N, Wang YT, Guo TT, Yang T, Chen ML, Wang JH (2016) Green preparation of carbon dots with papaya as carbon source for effective fluorescent sensing of Iron (III) and Escherichia coli. Biosens Bioelectron 85:68–75
62. Pappalardo JS, Macairan JR, Macina A, Poulhazan A, Quattrocchi V, Marcotte I, Naccache R (2020) Effects of polydopamine-passivation on the optical properties of carbon dots and its potential use in vivo. Phys Chem Chem Phys 22(29):16595–16605
63. Wang F, Chen NP, Li JR, Xu ZQ (2022) Chitosan microspheres loaded with 5Fu and polydopamine-carbon dots for enhancing chemo-photothermal therapy. Mater Lett 329:133167
64. Guo JZ, Li H, Ling LT, Li G, Cheng R, Lu X, Xie AQ, Li Q, Wang CF, Chen S (2020) Green synthesis of carbon dots toward anti-counterfeiting. Acs Sustain Chem Eng 8(3):1566–1572

65. Urbanová M, Pola J (2004) IR laser decomposition of 1,3-disilacyclobutane in presence of carbon disulfide: chemical vapour deposition of polythiacarbosilane. J Organomet Chem 689(16):2697–2701
66. Wang WJ, Wu J, Xing YX, Wang ZH (2022) Solvent-dependent red emissive carbon dots and their applications in sensing and solid-state luminescence. Sensors Actuators B-Chem 360:131645
67. Yu RS, Liang S, Ru Y, Li L, Wang ZK, Chen JL, Chen L (2022) A Facile Preparation of Multicolor Carbon Dots. Nanoscale Res Lett 17(1):32
68. Huang QQ, Bao QQ, Wu CY, Hu MR, Chen YN, Wang L, Chen WD (2022) Carbon dots derived from Poria cocos polysaccharide as an effective "on-off" fluorescence sensor for chromium (VI) detection. J Pharmaceutical Anal 12(1):104–112
69. Liu JJ, Li DW, Zhang K, Yang MX, Sun HC, Yang B (2018) One-step hydrothermal synthesis of nitrogen-doped conjugated carbonized polymer dots with 31% efficient red emission for in vivo imaging. Small 14(15):1703919
70. Ran QQ, Wang XP, Ling P, Yan PW, Xu J, Jiang L, Wang Y, Su S, Hu S, Xiang J (2022) A thermal-assisted electrochemical strategy to synthesize carbon dots with bimodal photoluminescence emission. Carbon 193:404–411
71. Xu XK, Mo LQ, Li YD, Pan XQ, Hu GQ, Lei BF, Zhang XJ, Zheng MT, Zhuang JL, Liu YL, Hu CF (2021) Construction of carbon dots with color-tunable aggregation-induced emission by nitrogen-induced intramolecular charge transfer. Adv Mater 33(49):2104872
72. Liang CZ, Xie XB, Shi QS, Feng J, Zhang DX, Huang XM (2022) Nitrogen/sulfur-doped dual-emission carbon dots with tunable fluorescence for ratiometric sensing of ferric ions and cell membrane imaging. Appl Surf Sci 572:151447
73. Xu XK, Mo LQ, Li W, Li YD, Lei BF, Zhang XJ, Zhuang JL, Hu CF, Liu YL (2021) Red, green and blue aggregation-induced emissive carbon dots. Chin Chem Lett 32(12):3927–3930
74. Huo Z, Xu W, Chen G, Wang Z, Xu S (2021) Surface-state triggered solvatochromism of carbonized polymer dot and its two-photon luminescence. Nano Res 15(3):2567–2575
75. Chen MX, Kobashi K, Chen B, Lu M, Tour JM (2010) Functionalized self-assembled InAs/GaAs quantum-dot structures hybridized with organic molecules. Adv Func Mater 20(3):469–475
76. Gigault J, El Hadri H, Nguyen B, Grassl B, Rowenczyk L, Tufenkji N, Feng SY, Wiesner M (2021) Nanoplastics are neither microplastics nor engineered nanoparticles. Nat Nanotechnol 16(5):501–507
77. Gao Y, Liu QF, Zeng YY, Li HY, Hu CQ, Wang C (2023) Synthesis of a novel microplastic trap with abundant oxime groups based on MOF-545 post-engineering for the environmental pollution control and water remediation. J Clean Prod 430:139678